Available online at www.sciencedirect.com
ScienceDirect
International Journal of Heat and Mass Transfer 50 (2007) 808–820
International Journal of HEAT and MASS TRANSFER
www.elsevier.com/locate/ijhmt

Heat and mass transfer in gas metal arc welding. Part II: The metal

J. Hu [1], H.L. Tsai *

Department of Mechanical and Aerospace Engineering, University of Missouri–Rolla, 1870 Miner Circle, Rolla, MO 65409, United States

Received 18 January 2006; received in revised form 22 August 2006
Available online 24 October 2006

Abstract

In this Part II, a thorough investigation of the melting of the electrode; the droplet formation, detachment, transfer and impingement onto the workpiece, and the weld-pool formation and dynamics was conducted. The transient melt-flow velocity and temperature distributions in the droplet and in the weld pool were calculated. The resulting crater in the weld pool and the weld-pool oscillation due to periodical droplet impingement were predicted. The solidification process in the electrode and in the weld pool after the current was turned off was also simulated. The predicted droplet flight trajectory is in good agreement with published data.
© 2006 Elsevier Ltd. All rights reserved.

Keywords: GMAW; Droplet formation; Droplet transfer; Droplet impingement; Weld pool dynamics

1. Introduction

In Part I [1] of this work, we presented the computational results of the plasma arc. The heat transfer and fluid flow in the arc at typical time instants have been presented to show the characteristics of the arc and the influence of the electrode shape, the droplet struck in the middle of the electrode and the workpiece, and the deformed weld pool shape on the arc-plasma flow. A unified model and its numerical solution schemes, which can calculate the arc-plasma generation; the melting of the electrode; the droplet formation, detachment, transfer, and impingement onto the workpiece; and the weld-pool dynamics, have also been presented in Part I [1]. In this Part II, we will present the results in the metal region, which include the electrode, the droplet between the electrode and the workpiece, and the weld pool. The heat transfer and fluid flow in the metal will be presented to study the melting of the electrode; the droplet formation, detachment, transfer, and impingement onto the workpiece; and the weld-pool dynamics.

Due to its high productivity, the GMAW process has been the predominant welding method. The welding quality depends on various parameters, such as welding current, electrode feed rate, travel speed, and shielding gas. A comprehensive dynamic model of the GMAW process would provide many helpful insights on key process parameters leading to the improvement of weld quality. In such a model, there are three major coupling events that need to be considered: (1) the generation and changing process of arc plasma, (2) the dynamic process of droplet formation, detachment, and impingement onto the weld pool, and (3) the dynamics of the welding pool under the influences of arc plasma and the periodical impingement of droplets. Due to the complexity of the welding process, many existing numerical models only focused on one or two events of the GMAW process while simplifying the rest of the events.

Much research in GMAW has been done to study droplet formation [2–15] and weld-pool dynamics [13–27], but very few works have been done to investigate the arc plasma and its influence on the metal transfer and

* Corresponding author. Tel.: +1 573 341 4945; fax: +1 573 341 4607.
E-mail address: tsai@umr.edu (H.L. Tsai).
[1] Present address: Department of Mechanical Engineering, University of Bridgeport, Bridgeport, CT 06604, United States.

0017-9310/$ - see front matter © 2006 Elsevier Ltd. All rights reserved.
doi:10.1016/j.ijheatmasstransfer.2006.08.026

weld-pool dynamics [7–14]. Choi et al. [2–4] have assumed both a uniform and a linear current density distribution on the droplet surface to compute the droplet surface profile and the velocity distribution in the droplet. Wang et al. [5] also have simulated the droplet surface profile and fluid flow in the droplet by assuming a Gaussian current distribution at the droplet surface. Fan and Kovacevic [15] and Wang et al. [6] simulated the heat transfer and fluid flow in the droplet by assuming linear current density distribution and heat flux distribution on the droplet surface. The metal transfer in the above models has been treated as an isolated process, within which the droplets were only subjected to surface tension, gravity force, and electromagnetic force calculated with a simplified current density distribution.

The heat transfer and fluid flow in a GMAW weld pool are similar to that in a GTAW weld pool, which have been extensively studied in the past several decades [28–36]. Without metal deposition onto the weld pool, the weld-pool surface has been considered as flat in these GTAW weld-pool models. However, the impingement of molten droplets onto the weld pool in GMAW greatly affects the shape of the free surface and the convective heat transfer in the weld pool. The deformed weld pool influences the current distribution in the arc and thus influences the heat and momentum fluxes transferred from the arc plasma to the weld pool. Modeling the dynamics of the weld pool in GMAW has been greatly simplified by many researchers [17–22] due to the complicated interactions among arc plasma, droplets, and workpiece. The weld pool was assumed to be a flat surface in the models of Tsao and Wu [17], Kumar and Bhaduri [18,19], and Jaidi and Dutta [27]. Using boundary fitted coordinates, weld-pool surface deformation has been incorporated into models by Kim and Na [20], Kim et al. [21], and Ohring and Lugt [22]. The dynamic change of the weld pool free surface was recently modeled by Wang and Tsai [24–26], and Fan and Kovacevic [14–16] using the VOF method and Cao et al. [23] using the FAVOR method. Many models only consider the heat transfer by conduction [19,21] or fluid flow [4] in the weld pool. Only recent models [13–17,22–26] have calculated both the heat transfer and fluid flow in the weld pool. The dynamic impingement of a droplet onto the weld pool has been omitted [20], treated as a liquid column [22] or cylindrical volumetric heat source [21] acting on the weld pool in many weld pool models. Wang and Tsai [24–26], Fan and Kovacevic [16], and Cao et al. [23] have simulated the dynamic interaction of a droplet impinging onto the weld pool including both heat transfer and fluid flow effects. However, they all assumed the droplets were already generated with a certain shape, volume, temperature, and initial velocity at a certain distance above the weld pool. The droplet then was accelerated to the weld pool by applying a drag force calculated from an empirical formula and an assumed plasma velocity. Fan and Kovacevic [15] developed a model to simulate the droplet formation, detachment, and impingement onto the molten pool without calculating the arc plasma and its effect on the metal region. However, this was essentially a model with three separate parts calculating droplet formation, transfer and impingement onto the weld pool. Linear current and heat flux distributions were assumed at the electrode surface. The plasma drag force was calculated from assumed plasma velocity, and Gaussian current density and heat flux distributions were assumed at the weld-pool surface.

Very few documents have been found modeling the heat transfer and fluid flow in the arc plasma column in GMAW [7–14,37]. There are even fewer documents found trying to simulate the interaction of the arc plasma with the melting electrode and workpiece. Zhu et al. [8] calculated the anode temperature profile by incorporating an arc model into a one-dimensional conduction model of the moving electrode. The heat input to the electrode was estimated from the arc plasma and the 'molten' metal was discarded when its temperature reached the melting point. Haidar and Lowke [9] and Haidar [7,10–12] used an arc model to simulate the droplet formation in GMAW. They were the first to simulate the dynamic interaction of the arc plasma and the droplet. However, the droplet was eliminated immediately when it was detached from the electrode tip. The weld-pool dynamics was also omitted and the workpiece was treated as a flat plate. The fluid flow in the weld pool was not calculated and only the heat conduction was considered. Zhu et al. [13] and Fan and Kovacevic [14] have developed models to simulate the arc column; the droplet formation, detachment, transfer, and impingement onto the workpiece; and the weld-pool dynamics. However, the simulated arc plasma distribution matched both the experimental results [38–40] and the simulation results from those of the published arc simulations [7–12,41–48] poorly. From the simulated fluid flow within the droplets in Ref. [13], the coupling of the arc plasma and the droplets seemed to be poor as the droplets showed very little sign of being subjected to the electromagnetic force, arc pressure, and plasma shear stress. The arc plasma flow in Ref. [14] could not push the detached droplets down and an empirical formulation was used to calculate the plasma drag force.

In almost all aforementioned studies, the interaction of arc plasma with electrode melting, droplet generation and transfer, and weld pool dynamics was not considered. Linear or Gaussian current density and heat flux were assumed at the electrode surface [2–6,15]. The momentum transfer from the arc plasma to the electrode surface was usually omitted [2–6,15]. Gaussian current density, heat flux, and arc pressure were usually assumed at the surface of the workpiece [15–26]. However, in reality, the surface of the workpiece is highly deformable, and the profile of the electrode changes rapidly, which greatly influence the arc plasma flow and thus change the current, heat flux and momentum distribution at the metal surface. Furthermore, the arc plasma can be dramatically distorted when there are free droplets between the electrode tip and the surface of the weld pool. The details of arc flow distortion by free droplets and deformed workpieces have been discussed in the first part of this paper [1]. In this article, we will focus

on the melting of the electrode; the droplet formation, detachment, transfer, and impingement onto the workpiece; and the weld-pool dynamics under the influence of the arc plasma. The mathematical model employing the volume of fluid (VOF) technique and the continuum formulation developed to simulate the coupled transport phenomena including the arc plasma; electrode melting; droplet formation, detachment, and impingement onto the workpiece; and the dynamics of the weld pool was presented in the first paper [1].

2. Results and discussion

The welding conditions and other parameters used in calculations are listed in Part I [1]. In this study, a 200 A current is applied to the electrode from 0 s to 1 s. A complete sequence of electrode melting; droplet formation, detachment, transfer, and impingement onto the workpiece; and weld-pool dynamics is calculated. However, in the following paragraphs, results will be presented for the first three droplets' formation, detachment, transfer, and impingement onto the workpiece, and weld-pool development; for the weld-pool dynamics after the impingement of the last droplet; and for the solidification process of the electrode and weld pool after the current is turned off. The corresponding temperature distributions in the metal, velocity distributions in the metal, and temperature distributions in both the arc plasma and the metal of these cases are shown in Figs. 2–4. In order to effectively illustrate the welding phenomena of interest, the time intervals between each figure are not equal. Also, in order to increase the readability of flow direction, only a quarter of the grid nodes were used in each velocity vector plot in Fig. 3.

To clearly illustrate the heat transfer and fluid flow within the droplet at the electrode tip, the distributions of temperature, velocity, electrical potential, current, and electromagnetic force within the droplet at $t = 100$ ms are drawn in Fig. 1. The metal transfer mode of a 1.6-mm diameter mild-steel electrode is globular transfer under a 220-A current. The shape of the droplet shown in Fig. 1 is round and is in agreement with the experimental results of Jones et al. [38–40]. Jones et al. [38–40] observed round droplets at the electrode tip for a current range of 200–260 A in their experiments conducted for a 1.6-mm diameter mild-steel electrode in Ar-2% O_2 environment. The temperature within the droplet is determined by the concentrated heating at the anode surface and the flow pattern within the droplet. As shown in Fig. 1(b), liquid metal near the centerline of the droplet moves downward and circulates upward along the surface. Thus a counter-clock wise flow forms within the droplet, which brings cooler fluid at the droplet root to the droplet bottom and brings heat at the bottom to the higher part of the droplet. The droplet surface is also cooled down by the evaporation heat loss of the metal. The highest temperature found at the droplet surface is 2936 K, which is in agreement with the experimental data of [49]. The fluid flow pattern within the droplet is caused by a balance of forces acting on the droplet, which includes electromagnetic force, surface tension force, gravity, arc pressure, and plasma shear stress. The electromagnetic force and current density are determined by the electrical potential distribution. As the electrical conductivity is high in the metal, less than 0.2 V of voltage drop is found within the droplet. The electrical potential contours are concave at the root of the droplet, showing current diverges from the solid electrode with a smaller radius into the round droplet with a bigger radius. The electrical potential contours within the droplet are almost flat and have a slightly concave shape in the upper part of the droplet and a slightly convex shape in the lower part. Current within the droplet flows mainly parallel to the axis and slightly diverges in the upper part of the droplet and converges in the lower part. Current flowing out of the

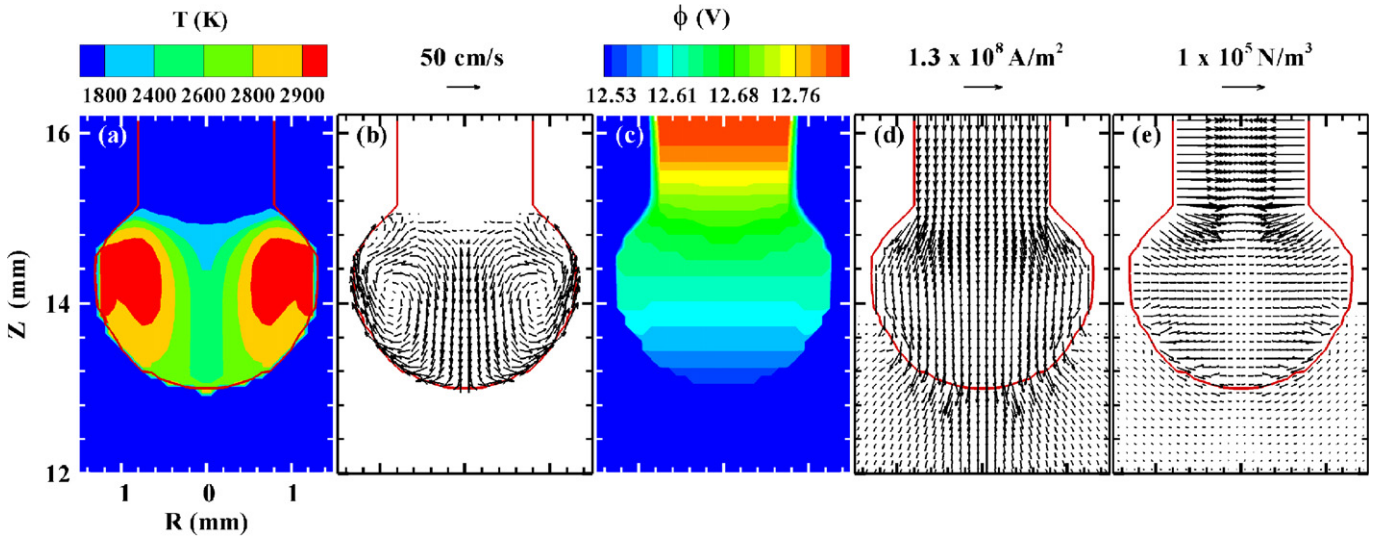

Fig. 1. Distribution of physical variables within the droplet at $t = 100$ ms. (a) Temperature; (b) velocity; (c) electrical potential; (d) current density; and (e) electromagnetic force.

droplet surface is mainly from the lower part of the droplet. The radial electromagnetic force is inward, which has a pinch effect on the droplet. The axial electromagnetic force is upward in the lower part of the droplet, where current converges, and downward in the upper part of the droplet, where current diverges. The maximum electromagnetic force is at the droplet surface, where the magnetic field has the highest value. The inward and downward electromagnetic force at the upper part of the droplet pushes the liquid metal downward at the center. The upward electromagnetic force, surface tension, and arc pressure hold the droplet at the bottom and change the fluid to flow upward along the surface. The pinch effect of the radially inward electromagnetic force, gravity, and plasma shear stress also help to cause the downward flow within the droplet.

The first droplet formation is shown in Figs. 2–4 from $t = 20$ ms to $t = 114$ ms. A round droplet forms at the electrode tip and grows bigger with a balance of electromagnetic force, surface tension force, gravity, arc pressure and plasma shear stress. After a neck is formed at $t = 114$ ms, the velocity within the droplet increases due to the increased electromagnetic pinch force at the neck. The droplet is detached and transferred to the workpiece from $t = 118$ ms to $t = 133$ ms. The detached droplet is accelerated by the plasma arc and gravity and reaches the workpiece with an axial velocity of about 60 cm/s.

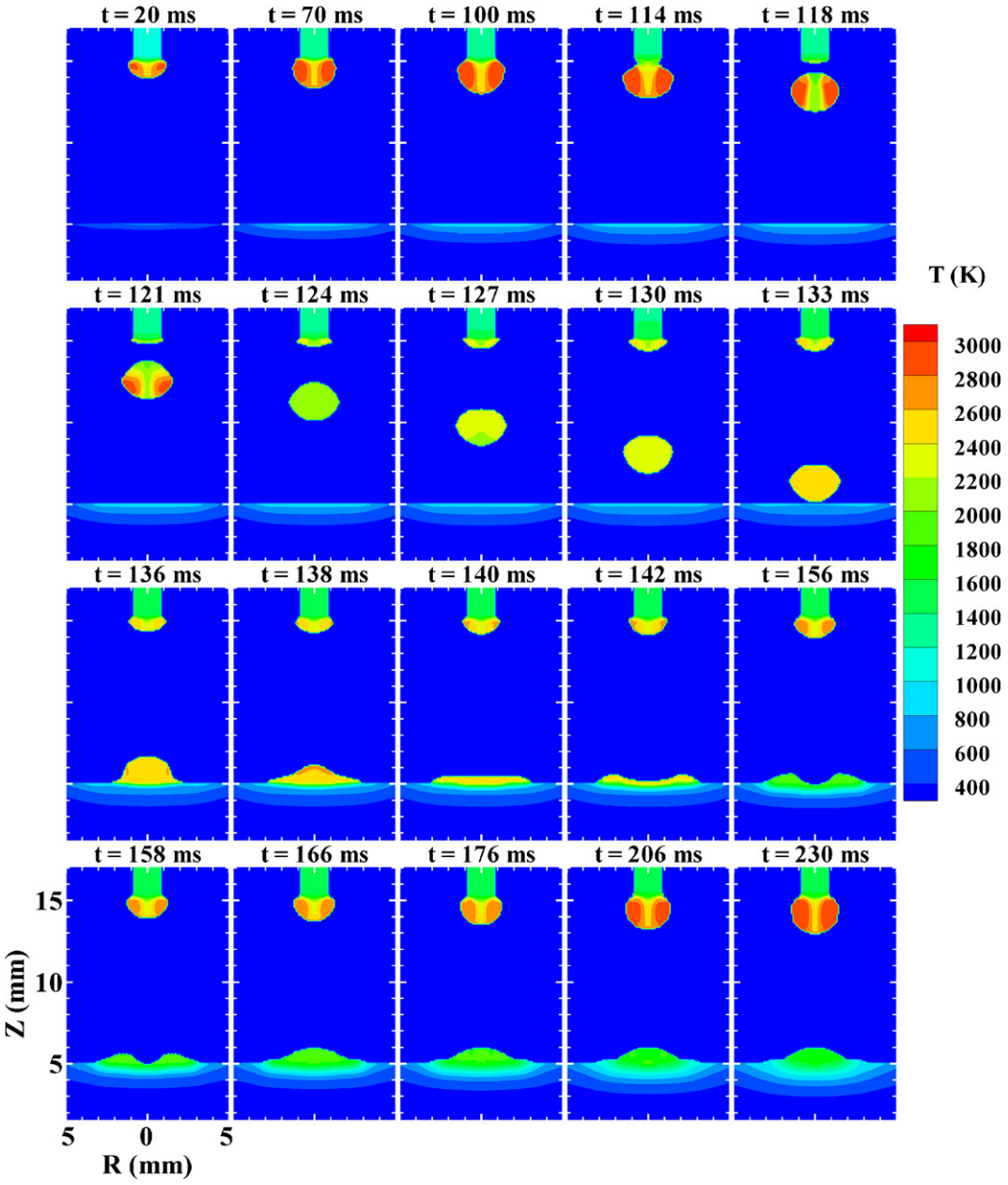

Fig. 2. A sequence of temperature distributions in the metal showing droplet generation, detachment, transfer in the arc, impingement onto the weld pool, and weld-pool dynamics.

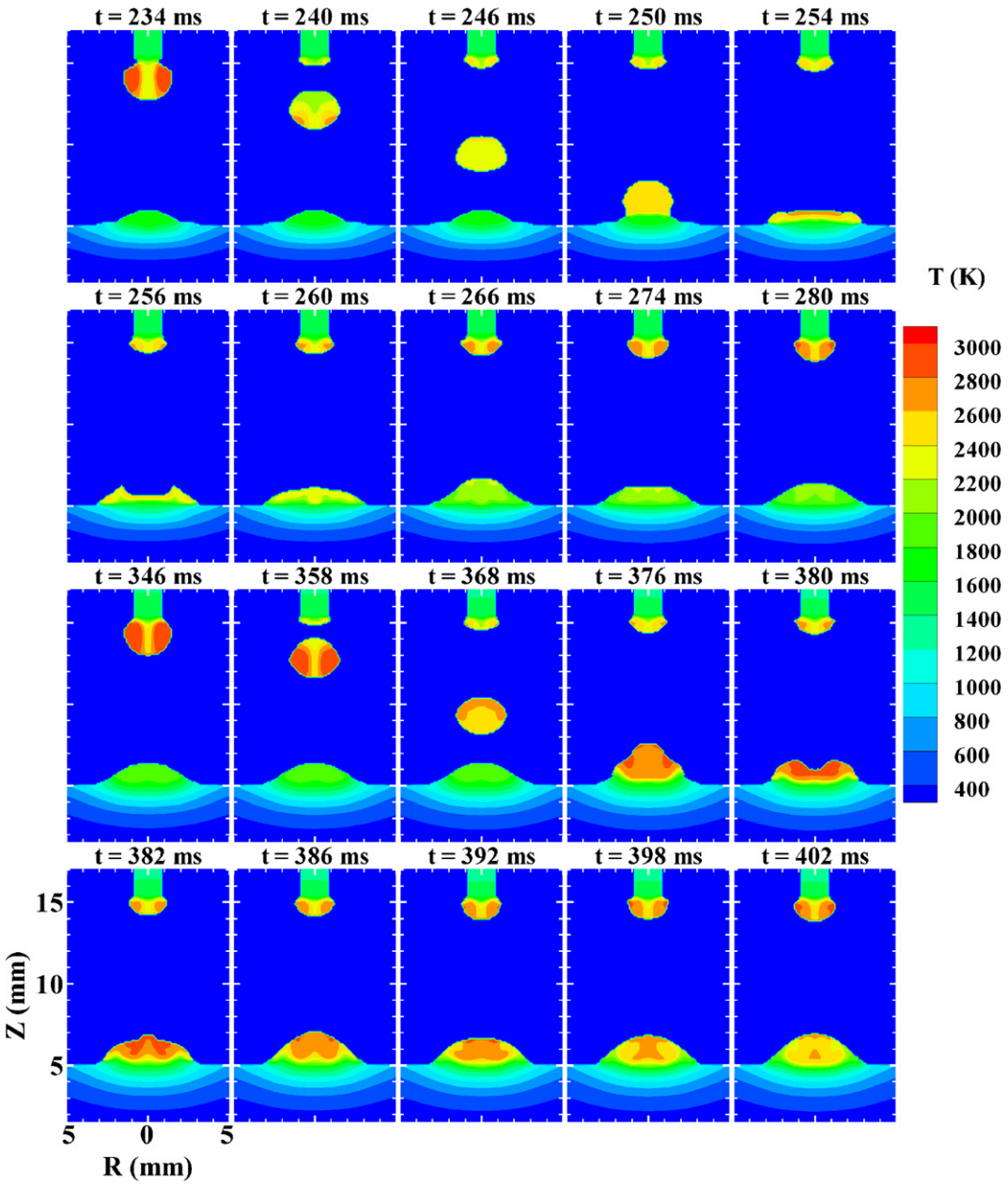

Fig. 2 (*continued*)

Subjected to the arc pressure, plasma shear stress, surface tension, and electromagnetic force, the detached droplet also changes its shape in the arc. The fluid flow in the detached droplet helps to mix the cold liquid in the droplet center with the hot liquid at the surface. Thus, a more uniform temperature distribution appears in the detached droplet than in the droplet hanging at the electrode tip. The detached droplet is continually heated by the surrounding high temperature plasma arc when it is accelerated toward the workpiece. Before the droplet impacts the workpiece, the workpiece has also been warmed by the arc plasma, but the surface temperature of the workpiece is still low. When the droplet hits the solid workpiece, it quickly spreads out on the workpiece from $t = 136$ to $t = 140$ ms. The droplet fluid is continually pushed downward and outward by arc pressure and arc shear stress from $t = 142$ ms to $t = 156$ ms. Some workpiece metal is melted by the superheated thermal energy contained by the droplet and mixes with the droplet. Thus, the mass, momentum, and thermal energy carried by the droplet mix and merge into the workpiece. A weld pool begins to form. The weld pool temperature continues to drop as it spreads outward and loses heat to the cold base metal by conduction. At $t = 156$ ms, the outer edge of the weld pool is already solidified. However, the center of the weld pool temperature is still substantially high and there is still fluid flow inside. From $t = 156$ ms to 166 ms, the fluid flow direction has been changed to inward by the surface tension force and hydrostatic force to fill the crater formed at the weld pool center. The temperature of the

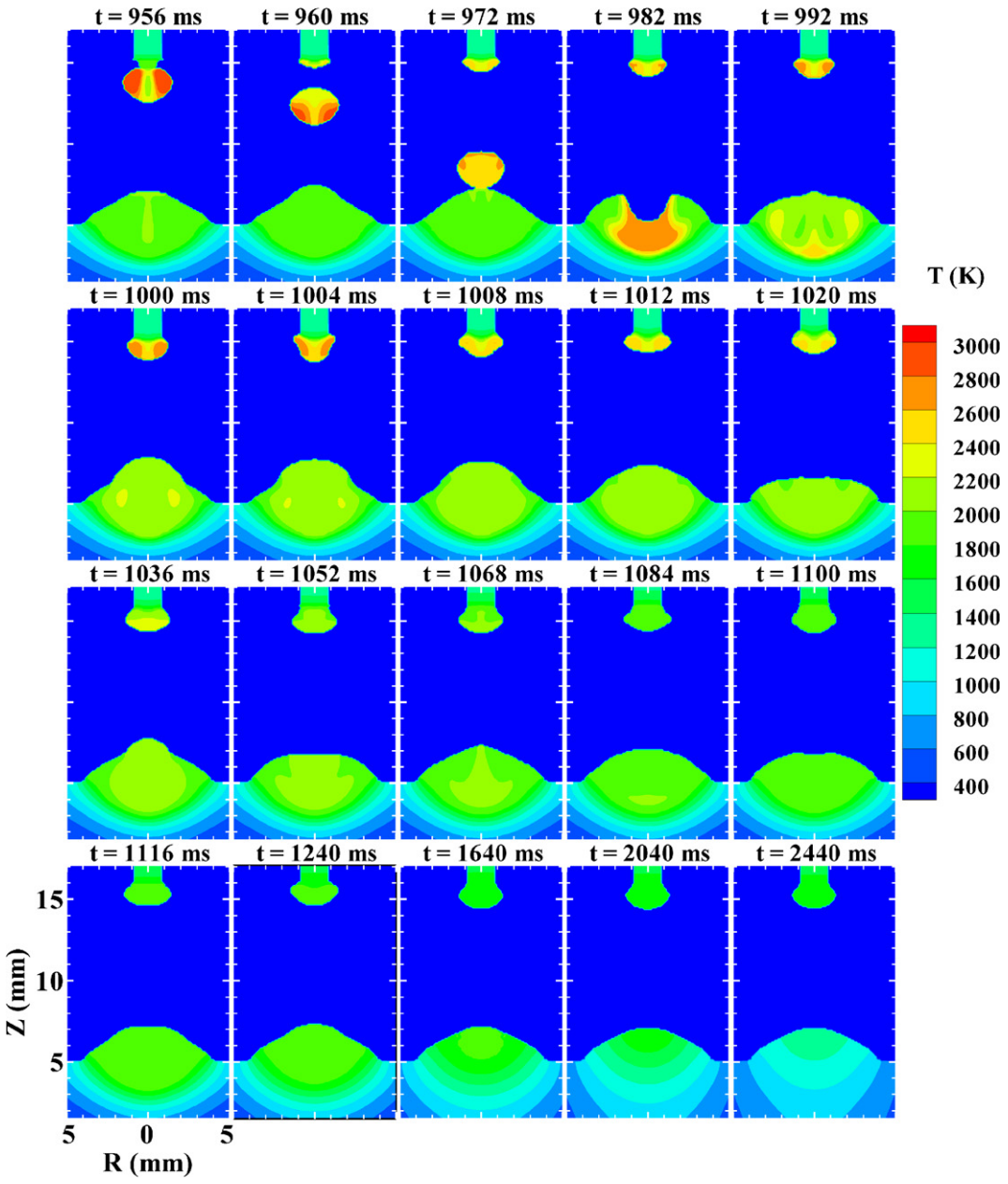

Fig. 2 (*continued*)

weld pool continues to decrease and so does the velocity in the weld pool. Before the second droplet impinges onto the weld pool at $t = 250$ ms, the weld pool is almost solidified.

After the first droplet is detached at $t = 118$ ms, the second droplet begins to form at the electrode tip. The second droplet necks, detaches, and is transferred to the weld pool from $t = 234$ ms to $t = 250$ ms. At $t = 250$ ms, the second droplet impinges onto the nearly solidified weld pool. Unlike the first droplet impinging onto a cold solid surface, the second superheated droplet quickly melts the preheated weld pool surface and penetrates into the weld pool center. The outward flow along the weld pool surface at the rim of the weld pool is quickly changed to an inward flow at $t = 254$ ms. A crater is formed at the weld-pool center by the downward momentum of the droplet and then it is filled up at $t = 260$ ms by surface tension and hydrostatic force. Affected by inertia, the fluid at the center continues to go upward and passes the equilibrium. The raised surface at the weld pool center is then pushed down by surface tension, arc pressure force, and hydrostatic force at $t = 274$ ms. The downward flow also passes the equilibrium, due to inertia, and rises up again at $t = 280$ ms. This loop continues until equilibrium is achieved and this process is called weld pool oscillation. The well-mixed weld pool continues to lose heat to the surrounding metal and the weld pool becomes smaller. By the time the third droplet reaches the weld pool surface at $t = 368$ ms, the edge of the weld pool has solidified. The third droplet impinges

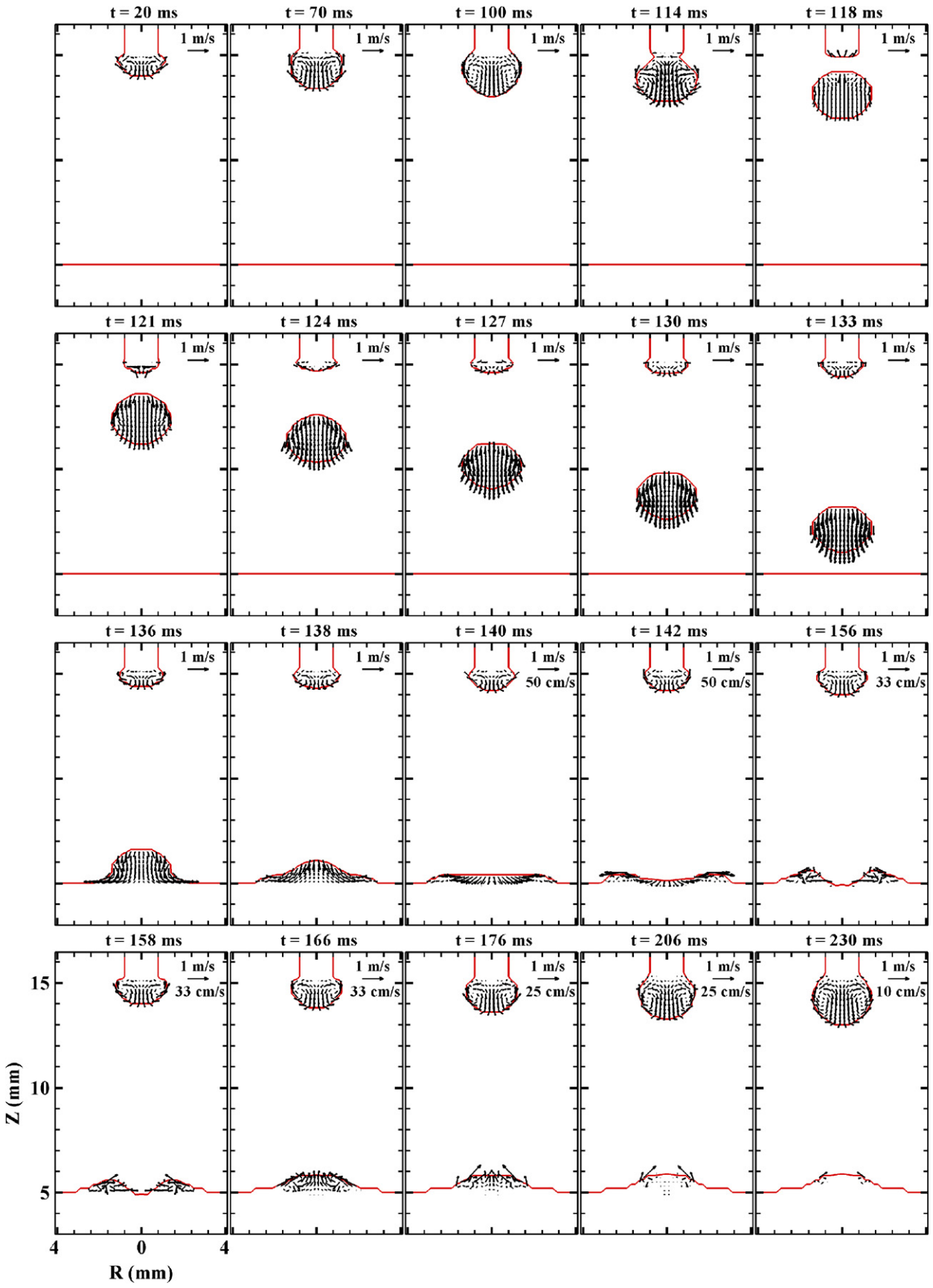

Fig. 3. The corresponding velocity distributions of the cases shown in Fig. 2.

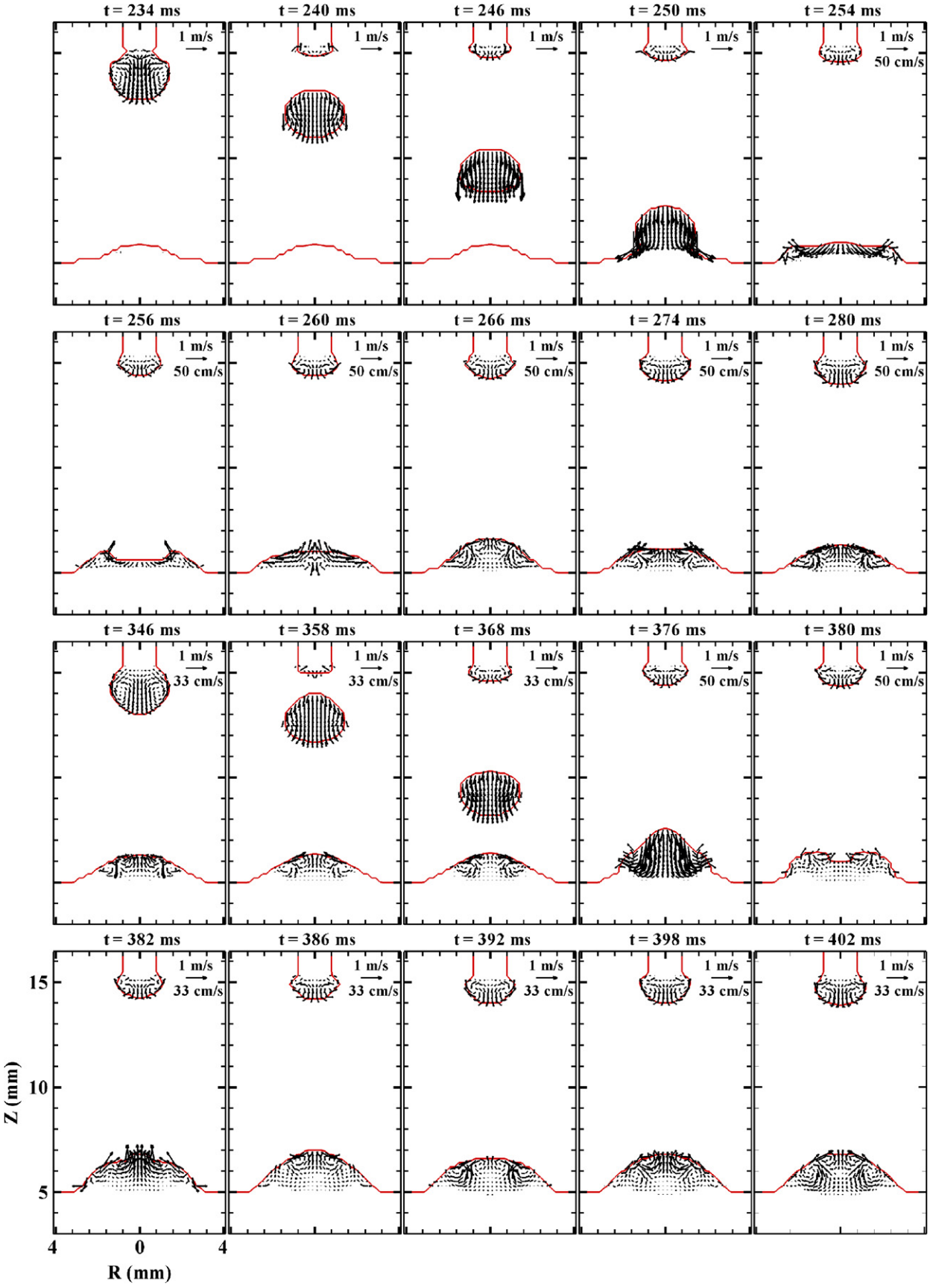

Fig. 3 (*continued*)

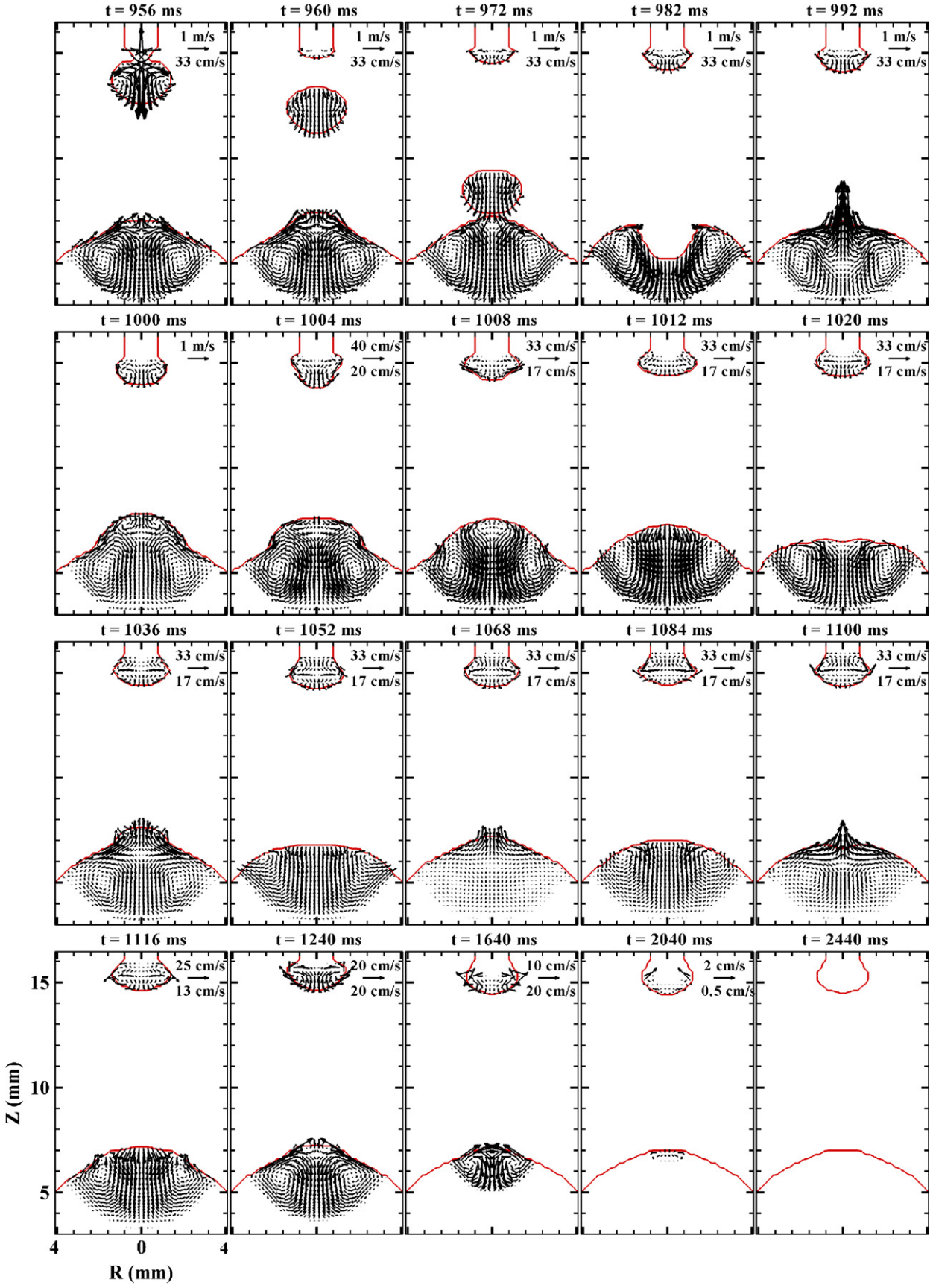

Fig. 3 (*continued*)

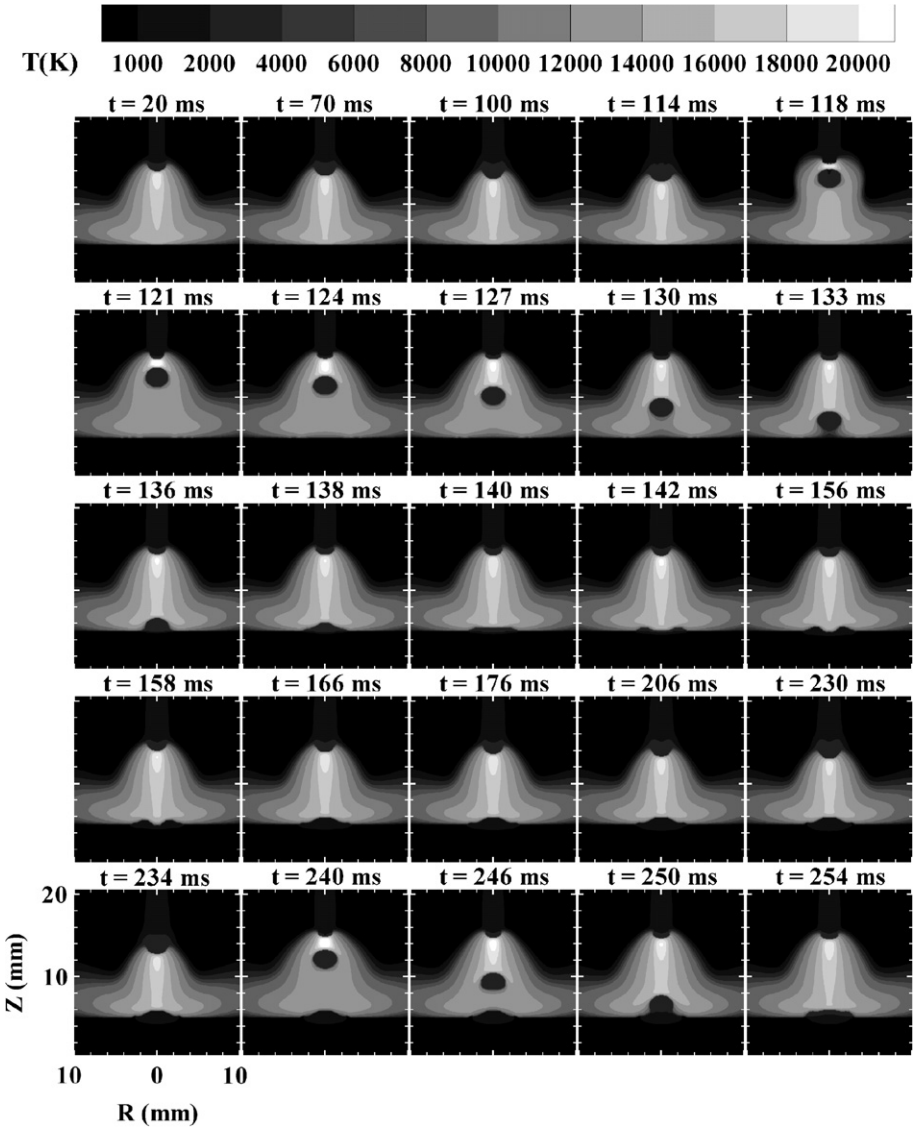

Fig. 4. The corresponding temperature distributions in both the arc and metal of the cases shown in Fig. 2.

onto the liquid weld pool and the downward momentum causes a bigger crater and stronger oscillation in the weld pool than the second droplet did. From $t = 380$ ms to $t = 402$ ms, the up-and-down motion of the weld pool can be seen more clearly than it was after the impingement of the second droplet. After three droplets are deposited onto the weld pool, the weld pool becomes bigger and the penetration becomes deeper.

At $t = 956$ ms, the ninth droplet is going to be detached from the electrode tip. The weld pool at the bottom is much bigger compared with the weld pool at $t = 402$ ms after the impingement of the third droplet. However, the flow patterns of the two figures are very similar. Both weld pools have downward flow at the center and inward flow at the weld-pool surface. The inward flow driven by surface tension at the weld-pool surface helps to form a downward flow at the weld-pool center and thus a counter-clock wise vortex at the weld pool edge. The ninth droplet is the last droplet simulated in this calculation. It should be noted that there was a substantial rise of fluid flow at the weld-pool center after the last droplet is detached at $t = 960$ ms. The rise of flow is caused by the decrease of arc pressure at the weld-pool surface when a droplet is stuck between the electrode tip and the weld pool, which has been explained in detail in Part I [1]. A bigger crater is formed after the last droplet impinges onto the bigger weld pool at $t = 982$ ms. The high-temperature filler metal carried by the droplet reaches the bottom of the weld pool, as shown in Fig. 2, at $t = 982$ ms. The big crater is then filled up by the surrounding fluid, and the weld pool first oscillates at high amplitude, then the oscillation gradually subsides. A sequence of experimental images were given

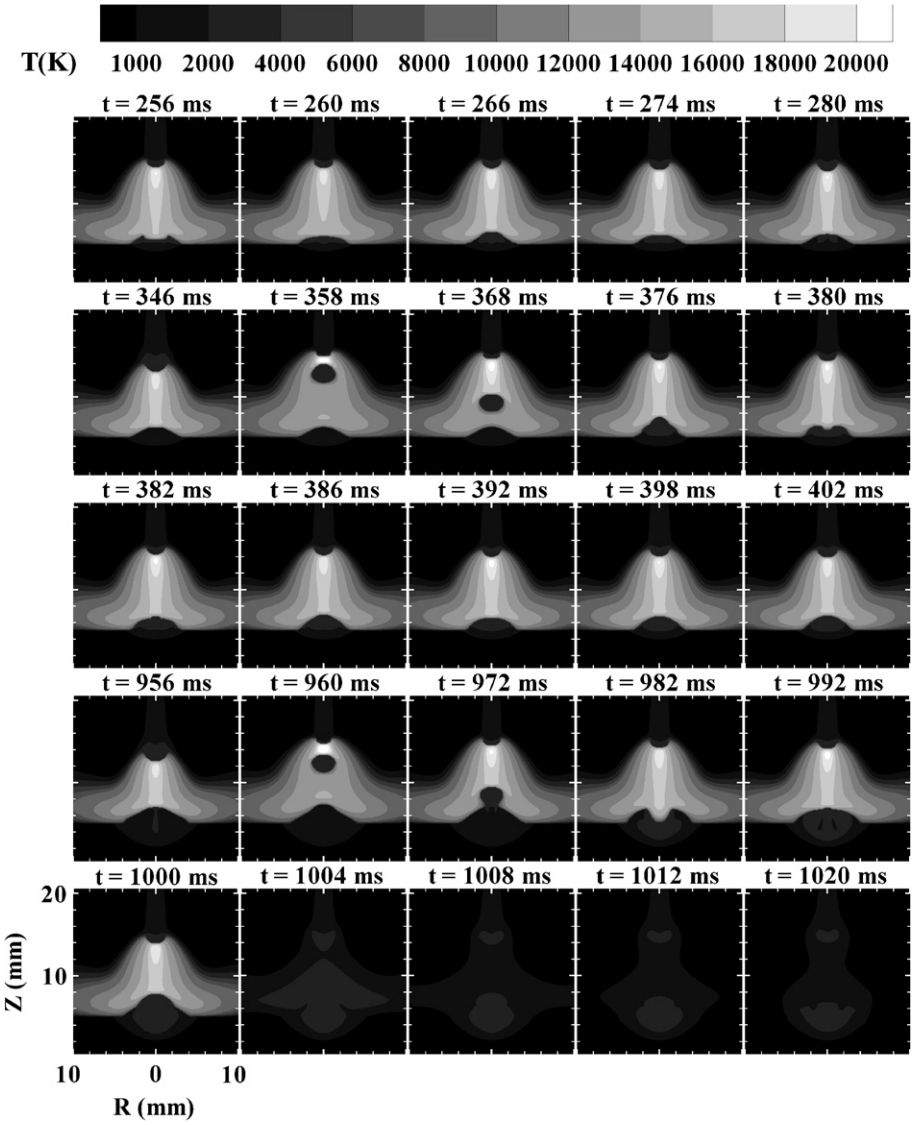

Fig. 4 (*continued*)

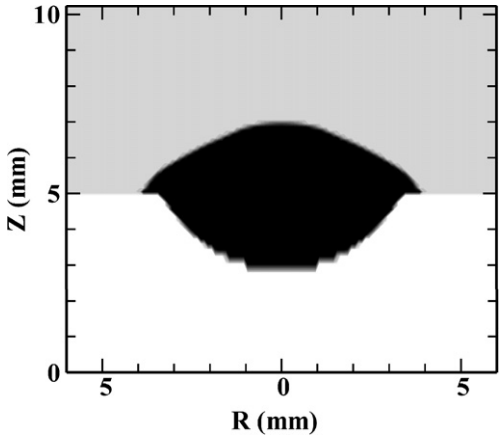

Fig. 5. The solidified weld-bead shape.

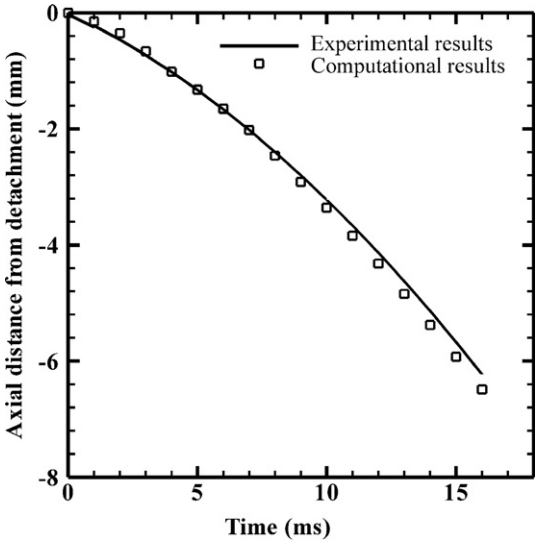

Fig. 6. Comparison of droplet flight trajectory with experiment results [40].

in Ref. [14] showing the weld-pool oscillation after a droplet impinges onto the weld pool, which can be seen by the up-and-down movement of the weld pool surface.

The current applied to the electrode dropped to 0 at $t = 1000$ ms. Due to the high radiation loss and low heat capacity of the arc plasma, the temperature in the arc plasma rapidly decreases without the Joule heating source from the current flow. At $t = 1004$ ms, the arc plasma temperature has become comparable to that of the weld pool and it continues to drop. The high-velocity arc plasma jet flow driven by the electromagnetic force also quickly dies down. Thus, the heat input from the arc to the metal surface and the arc pressure and plasma shear stress acting on the metal surface are gone immediately when the current is turned off. The electrode and weld pool begin to lose heat to the surrounding environment by radiation, convection, and conduction.

The weld pool continues to oscillate after the current is turned off, and the oscillation amplitude decreases as time increases. However, the fluid flow at the electrode tip changes dramatically when the arc pressure, plasma shear stress, and electromagnetic force are gone. At $t = 1004$ ms, the fluid flow at the bottom of the droplet supported by the arc pressure and surface tension flows downward when the arc pressure dramatically decreases. At the same time, the fluid at the droplet root flows upward along the electrode surface when the inward and downward electromagnetic force is gone. The droplet becomes elongated. The greatly distorted droplet shape causes a strong surface tension force, which rebounds the hot fluid at the bottom to flow upward and oblate the droplet at $t = 1008$ ms. The hot fluid at the bottom is then brought up to melt the electrode metal at the droplet root. The droplet continues to change its shape and oscillate at the tip of the electrode. The oscillation helps to mix the molten metal in the droplet and bring the hot fluid at the bottom upward to melt more electrode metal at the droplet root. Thus, the droplet becomes bigger and the solid and liquid interface moves up in the electrode.

Due to the heat loss to the solid metal by conduction and to the surroundings by radiation and convection, the sizes of the molten droplet and the weld pool become smaller. As the heat loss occurs mainly through conduction to the solid metal, the liquid metal adjacent to the solid and liquid interface solidifies first. The last liquid zone in the electrode is in the tip of the electrode and the last liquid zone in the weld pool is on the top of the weld pool. The solidification in the electrode is complete at $t = 2600$ ms and in the weld pool at $t = 2440$ ms. Fig. 5 shows the final shape of the weld bead including weld penetration which is similar to the reported experimental results [14–16].

To compare with the flight trajectory taken by Jones et al. [40], the center positions of the first detached droplet shown in Fig. 2 were plotted as a function of time. As can be seen in Fig. 6, the droplet trajectory from the computation matches the experimental results. Adopting the same method of Jones et al. [40] to calculate droplet acceleration, the droplet trajectory is fitted with a quadratic curve and the acceleration is then obtained by taking the second derivative of the curve. In this way, the acceleration of the detached is found to be 24 m/s^2, which is comparable to 21 m/s^2 obtained by Jones et al. [40].

3. Conclusions

Using a unified gas–metal arc welding model, the melting of the electrode; the droplet formation, detachment, transfer, and impingement onto the workpiece; and the weld-pool dynamics are simulated. Complicated fluid flow and heat transfer in the electrode, detached droplet and weld pool under the influence of the plasma arc are studied. No assumption of current density, heat flux, or arc pressure is assumed at the droplet and workpiece surface. The current distribution is calculated through the coupling effect of the arc and the metal. The heat flux, arc pressure, and plasma shear stress are all obtained from the coupled arc domain. The solidification process of the electrode and weld pool is investigated after the arc is extinguished.

Acknowledgement

This work was partially supported by GM R & D center which is gratefully acknowledged.

References

[1] J. Hu, H.L. Tsai, Heat and mass transfer in gas metal arc welding, Part I: the arc, Int. J. Heat Mass Transfer, in press, doi:10.1016/j.ijheatmasstransfer.2006.08.025.
[2] S.K. Choi, C.D. Yoo, Y.-S. Kim, The dynamic analysis of metal transfer in pulsed current gas metal arc welding, J. Phys. D: Appl. Phys. 31 (1998) 207–215.
[3] S.K. Choi, C.D. Yoo, Y.-S. Kim, Dynamic simulation of metal transfer in GMAW, Part 1: globular and spray transfer modes, Weld. J. (1998) 38s–44s.
[4] S.K. Choi, C.D. Yoo, Y.-S. Kim, Dynamic simulation of metal transfer in GMAW, Part 2: short-circuit transfer mode, Weld. J. (1998) 45s–51s.
[5] G. Wang, P.G. Huang, Y.M. Zhang, Numerical analysis of metal transfer in gas metal arc welding, Metall. Trans. 34B (2003) 345–353.
[6] F. Wang, W.K. Hou, S.J. Hu, E. Kannatey-Asibu, W.W. Schultz, P.C. Wang, Modelling and analysis of metal transfer in gas metal arc welding, J. Phys. D: Appl. Phys. 36 (2003) 1143–1152.
[7] J. Haidar, A theoretical model for gas metal arc welding and gas tungsten arc welding. I, J. Appl. Phys. 84 (7) (1998) 3518–3529.
[8] P. Zhu, M. Rados, S.W. Simpson, A theoretical study of gas metal arc welding system, Plasma Sources Sci. Technol. 4 (1995) 495–500.
[9] J. Haidar, J.J. Lowke, Predictions of metal droplet formation in arc welding, J. Phys. D: Appl. Phys. 29 (1996) 2951–2960.
[10] J. Haidar, An analysis of the formation of metal droplets in arc welding, J. Phys. D: Appl. Phys. 31 (1998) 1233–1244.
[11] J. Haidar, Prediction of metal droplet formation in gas metal arc welding. II, J. Appl. Phys. 84 (7) (1998) 3530–3540.
[12] J. Haidar, An analysis of heat transfer and fume production in gas metal arc welding. III, J. Appl. Phys. 85 (7) (1998) 3448–3459.
[13] F.L. Zhu, H.L. Tsai, S.P. Marin, P.C. Wang, A comprehensive model on the transport phenomena during gas metal arc welding process, Prog. Comput. Fluid Dynamics 4 (2) (2004) 99–117.

[14] H.G. Fan, R. Kovacevic, A unified model of transport phenomena in gas metal arc welding including electrode, arc plasma and molten pool, J. Phys. D: Appl. Phys. 37 (2004) 2531–2544.
[15] H.G. Fan, R. Kovacevic, Droplet formation, detachment, and impingement on the molten pool in gas metal arc welding, Metall. Trans. 30B (1999) 791–801.
[16] H.G. Fan, R. Kovacevic, Dynamic analysis of globular metal transfer in gas metal arc welding – a comparison of numerical and experimental results, J. Phys. D: Appl. Phys. 31 (1998) 2929–2941.
[17] K.C. Tsao, C.S. Wu, Fluid flow and heat transfer in GMA weld pools, Weld. J. (March) (1988) 70s–75s.
[18] S. Kumar, S.C. Bhaduri, Three-dimensional finite element modeling of gas metal-arc welding, Metall. Trans. 25B (1994) 435–441.
[19] S. Kumar, S.C. Bhaduri, Theoretical investigation of penetration characteristics in gas metal-arc welding using finite element method, Metall. Trans. 26B (1994) 611–624.
[20] S.-D. Kim, S.-J. Na, A study on the effect of constant tube-to-workpiece distance on weld pool shape in gas metal arc welding, Weld. J. 74 (5) 141s–152s.
[21] C.-H. Kim, W. Zhang, T. DebRoy, Modeling of temperature field and solidified surface profile during gas–metal arc fillet welding, J. Appl. Phys. 94 (2003) 2667–2679.
[22] S. Ohring, H.J. Lugt, Numerical simulation of a time-dependent 3-D GMA weld pool due to a moving arc, Weld. J. (1999) 416s–424s.
[23] Z. Cao, Z. Yang, X.L. Chen, Three-dimensional simulation of transient GMA weld pool with free surface, Weld. J. (2004) 169s–176s.
[24] Y. Wang, H.L. Tsai, Impingement of filler droplets and weld pool dynamics during gas metal arc welding process, Int. J. Heat Mass Transfer 44 (2001) 2067–2080.
[25] Y. Wang, Q. Shi, H.L. Tsai, Modeling of the effects of surface-active elements on flow patterns and weld penetration, Metall. Trans. 32B (2001) 145–161.
[26] Y. Wang, H.L. Tsai, Effects of surface active elements on weld pool fluid flow and weld penetration in gas metal arc welding, Metall. Trans. 32B (2001) 501–515.
[27] J. Jaidi, P. Dutta, Modeling of transport phenomena in a gas metal arc welding process, Numer. Heat Transfer A 40 (2001) 543–562.
[28] P. Dutta, Y. Joshi, R. Janaswami, Thermal modelling of GTAW process with nonaxisymmetric boundary conditions, Numer. Heat Transfer A 27 (1995) 499–518.
[29] N. Chakraborty, S. Chakraborty, P. Dutta, Three-dimensional modeling of turbulent weld pool convection in GTAW processes, Numer. Heat Transfer A 45 (2004) 391–413.
[30] A.A. Reddy, B. Guha, D.R.G. Achar, Finite element modeling of three-dimensional transient heat transfer in stainless steel (304) pulsed GTA weldments, Numer. Heat Transfer A 41 (2002) 41–64.
[31] W.H. Kim, H.G. Fan, S.J. Na, Effect of various driving forces on heat and mass transfer in arc welding, Numer. Heat Transfer A 32 (6) 633–652.
[32] G.M. Oreper, J. Szekely, Heat and fluid-flow phenomena in weld pools, J. Fluid Mech. 147 (1984) 53–79.
[33] Y. Joshi, P. Dutta, D. Espinosa, P. Schupp, Non-axisymmetric convection in stationary gas tungsten arc weld pools, Trans. ASME, J. Heat Transfer 119 (1997) 164–171.
[34] M. Kanouff, R. Greif, The unsteady development of a GTA weld pool, Int. J. Heat Mass Transfer 35 (1992) 967–979.
[35] K. Mundra, T. Debroy, T. Zacharia, S. David, Role of thermophysical properties in weld pool modeling, Weld. J. 71 (1992) 313–320.
[36] R.T.C. Chao, J. Szekely, The possible role of turbulence in GTA weld pool behavior, Weld. J. 73 (1994) 25–31.
[37] P.G. Jonsson, R.C. Westhoff, J. Szekely, Arc characteristics in gas-metal arc welding of aluminum using argon as the shielding gas, J. Appl. Phys. 74 (1993) 5997–6006.
[38] L.A. Jones, T.W. Eagar, J.H. Lang, Images of steel electrode in Ar-2% O_2 shielding during constant current gas metal arc welding, Weld. J. (1998) 135s–141s.
[39] L.A. Jones, T.W. Eagar, J.H. Lang, Magnetic forces acting on molten drops in gas metal arc welding, J. Phys. D: Appl. Phys. 31 (1998) 93–106.
[40] L.A. Jones, T.W. Eagar, J.H. Lang, A dynamic model of drops detaching from a gas metal arc welding electrode, J. Phys. D: Appl. Phys. 31 (1998) 107–123.
[41] J. Mckelliget, J. Szekely, Heat transfer and fluid flow in the welding arc, Metall. Trans. 17A (1986) 1139–1148.
[42] R.T.C. Choo, J. Szekely, R.C. Westhoff, On the calculation of the free surface temperature of gas-tungsten-arc weld pools from first principles: part I. Modeling the welding arc, Metall. Trans. 23B (1992) 357–369.
[43] M. Goodarzi, R. Choo, J.M. Toguri, The effect of the cathode tip angle on the GTAW arc and weld pool: I. Mathematical model of the arc, J. Phys. D: Appl. Phys. 30 (1997) 2744–2756.
[44] H.G. Fan, Y.W. Shi, Numerical simulation of the arc pressure in gas tungsten arc welding, J. Mater. Process. Tech. 61 (1996) 302–308.
[45] P. Zhu, J.J. Jowke, R. Morrow, A unified theory of free burning arcs, cathode sheaths and cathodes, J. Phys. D: Appl. Phys. 25 (1992) 1221–1230.
[46] R.J. Ducharme, P.D. Kapadia, J. Dowden, I.M. Richardson, M.F. Thornton, A mathematical model of TIG electric arcs operating in the hyperbaric range, J. Phys. D: Appl. Phys. 29 (1996) 2650–2658.
[47] J. Menart, J. Heberlein, E. Pfender, Theoretical radiative transport results for a free-burning arc using a line-by-line technique, J. Phys. D: Appl. Phys. 32 (1999) 55–63.
[48] H.P. Schmidt, G. Speckhofer, Experimental and theoretical investigation of high-pressure arcs-Part I: the cylindrical arc column (two-dimensional modeling), IEEE Trans. Plasma Sci. 24 (1996) 1229–1238.
[49] J.F. Lancaster, The physics of welding, second ed., Pergamon, Oxford, 1986.